THE JOURNAL OF PHYSICAL CHEMISTRY A
A JOURNAL OF THE AMERICAN CHEMICAL SOCIETY

pubs.acs.org/JPCA Article

Gradient Bundle Analysis of Electric Field Induced Changes in Electron Charge Density

Published as part of The Journal of Physical Chemistry virtual special issue "Early-Career and Emerging Researchers in Physical Chemistry Volume 2".

Logan Epperson, Megan Mascarenas, and Amanda Morgenstern*

Cite This: *J. Phys. Chem. A* 2023, 127, 4682–4694 Read Online

ACCESS | Metrics & More | Article Recommendations | Supporting Information

ABSTRACT: Applying an electric field (EF) to a molecule is known to induce rearrangement of its electron charge density, $\rho(\mathbf{r})$. Previous experimental and computational studies have investigated effects on reactivity by using homogeneous EFs with specific magnitudes and directions to control reaction rates and product selectivity. To best incorporate EFs into experimental design, a more fundamental understanding of how EFs rearrange $\rho(\mathbf{r})$ is necessary. To gain this understanding, we first applied EFs to a set of 10 diatomic and linear triatomic molecules with various constraints on the molecules to determine the importance of rotation and altering bond lengths on bond energies. In order to capture the subtle changes in $\rho(\mathbf{r})$ known to occur from EFs, an extension of the quantum theory of atoms in molecules called gradient bundle (GB) analysis was employed, allowing for quantification of the redistribution of $\rho(\mathbf{r})$ within atomic basins. This allowed us to calculate GB-condensed EF-induced densities using conceptual density functional theory. Results were interpreted considering relationships between the GB-condensed EF-induced densities and properties including bond strength, bond length, polarity, polarizability, and frontier molecular orbitals (FMOs).

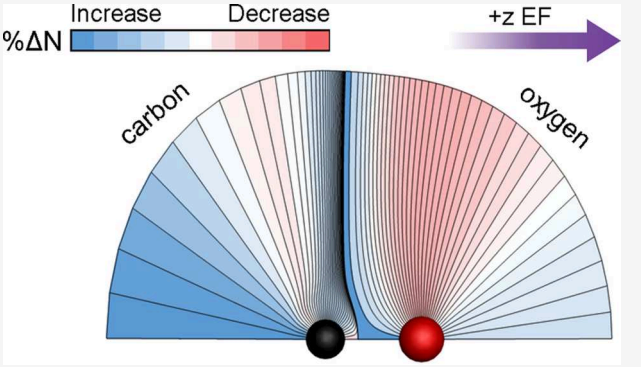

INTRODUCTION

Properly oriented electric fields (EFs) have recently been shown to be capable of controlling the rates of chemical reactions and the specific structures of products that are formed during reactions. These studies have been performed both computationally[1−9] and experimentally.[10−18] A frequent term in EF-driven catalysis coined by Shaik et al. is the reaction axis, which is defined as the direction in which a homogeneous EF should be applied to control reactivity such that the subsequent electron reorganization stabilizes a transition state (TS) or preferentially forms a specific product.[1,7] A homogeneous EF will generally move electrons in the direction of the field, but there is rearrangement of electron charge density, $\rho(\mathbf{r})$, that occurs in addition to this overall one-dimensional movement of electrons. While the energetic changes incurred by EFs can be substantial, the changes to $\rho(\mathbf{r})$ often appear to be more subtle.[19−21] In this work, we propose a method to create a general description of the exact rearrangement of $\rho(\mathbf{r})$ occurring due to an EF. The redistribution of $\rho(\mathbf{r})$ is investigated with gradient bundle (GB) analysis, an extension of the quantum theory of atoms in molecules (QTAIM).

Investigations of $\rho(\mathbf{r})$ with QTAIM and EFs have revealed how electrons transfer between atomic basins, volumes bounded by zero-flux surfaces (ZFSs) in the gradient field of the charge density, $\nabla\rho(\mathbf{r})$, which correspond to each atom in a molecule.[21,22] However, in addition to transferring electrons between atoms, EFs can significantly rearrange $\rho(\mathbf{r})$ within atomic basins. Furthermore, the changes occurring between atomic basins may or may not be representative of the overall changes in chemical reactivity. For example, Clarys et al. demonstrated that atomic charges of diatomic molecules do not change at all when homogeneous EFs are applied perpendicular to the bond, despite plots of the EF-induced charge density indicating significant changes in $\rho(\mathbf{r})$.[19] Similarly, Wilson et al. calculated the change in the number of electrons in bond wedges as well as atomic basins due to EFs in ketosteroid isomerase.[20] Bond wedges are volumes

Received: March 15, 2023
Revised: May 1, 2023
Published: May 18, 2023

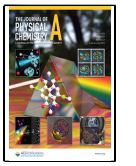

bounded by ZFSs in the bonding regions of atomic basins. It was shown that the amount of $\rho(\mathbf{r})$ lost and gained in bond wedges was often more significant than the overall change in atomic charge calculated from the entire atomic basin. While bond wedge electron counts provide a more detailed picture than atomic charges, this model still does not capture all of the redistribution of $\rho(\mathbf{r})$ that occurs in molecules due to EFs. Attempts at describing changes to $\rho(\mathbf{r})$ due to EFs have been made by overlaying contour plots of $\rho(\mathbf{r})$,[21] measuring changes in distance of specific $\rho(\mathbf{r})$ isosurfaces from nuclei,[19] and calculating the curvature of $\rho(\mathbf{r})$ isosurfaces.[23,24]

We further quantify the redistribution of $\rho(\mathbf{r})$ due to EFs using a set of 10 diatomic and linear triatomic molecules. We first show how bond energies change due to EFs for both the case where nuclei are fixed in place and the case where they are allowed to move with various levels of geometry constraints. Based on these results, we use primarily fixed-nuclei calculations moving forward, which is in line with the conceptual density functional theory (CDFT) definition of the EF-induced density.[19] We then describe general trends in the GB-condensed induced density before comparing the rearrangement of $\rho(\mathbf{r})$ due to EFs to Fukui functions, which show how $\rho(\mathbf{r})$ rearranges due to adding or removing electrons from a system.[25−27] Since homogeneous EFs applied along the bond of a diatomic molecule will generally increase the atomic charge in one atom and decrease the charge in the other, one might assume that these results would be similar to Fukui functions. However, we show that electron rearrangement from these two different types of perturbations are distinct.

We hope that these developments in the fundamental understanding of how EFs redistribute $\rho(\mathbf{r})$ will aid in the incorporation of EFs in experimental design for catalysis and product selectivity. Specifically, the exact determination of the reaction axis for a given system is not always straightforward. We aim to develop a model capable of predicting the EF direction best suited for altering reactivity. The first step in this process is quantifying the redistribution of electrons due to EFs.

THEORY AND COMPUTATIONAL METHODS

Gradient Bundles. In QTAIM, an atomic basin is defined as the volume bounded by unique ZFSs in $\nabla\rho(\mathbf{r})$ around each nucleus, allowing for quantum-mechanically well-defined properties to be integrated over these basins.[28−30] While atomic basins have unique ZFSs bounding them, these are not the only ZFSs in $\nabla\rho(\mathbf{r})$ if surfaces intersecting nuclei are included.[31−36] QTAIM analysis of the full atomic basin provides information about the overall region surrounding an atom, such as atomic charge and atomic energy, but does not account for changes happening *within* atomic basins. However, atomic basins can be further partitioned into smaller volumes still bounded by ZFSs. These smaller volumes, called gradient bundles, also have quantum-mechanically well-defined properties. GBs thus allow for finer analysis of how $\rho(\mathbf{r})$ is distributed throughout the atomic basin.[34,37−40]

GBs can be created using a variety of methods depending on available $\rho(\mathbf{r})$ data and the symmetry of the molecules studied.[40] Rotational GBs can be created for linear molecules and have the advantage of being simple to analyze with 1D plots. To create rotational GBs, gradient paths are seeded from equally spaced points on a small semicircle on a cut plane of $\rho(\mathbf{r})$ centered at a nuclear critical point. Due to the symmetry of linear molecules, a 360° rotation of these gradient paths about the internuclear axis creates ZFSs that bound the GBs. Details on this method are provided elsewhere.[34] This work studies linear molecules to take advantage of the ease of analysis of rotational GBs.

Conceptual Density Functional Theory. CDFT defines chemical properties in terms of partial derivatives of energy, E. This theory originally focused on derivatives taken with respect to the number of electrons, N, and the external potential, $v(\mathbf{r})$.[41−43] Important to this work, the Fukui function is defined as

$$f(\mathbf{r}) = \left(\frac{\partial^2 E}{\partial N \delta v(\mathbf{r})}\right) = \left(\frac{\partial \mu}{\delta v(\mathbf{r})}\right)_N = \left(\frac{\partial \rho(\mathbf{r})}{\partial N}\right)_{v(\mathbf{r})} \tag{1}$$

where μ is the chemical potential. The Fukui function is generally determined using a finite difference method where an electron is either added to or removed from the system ($\Delta N = \pm 1$), providing information on where nucleophilic or electrophilic attack is most likely to take place within a chemical system.[25−27] Furthermore, Fukui functions can be condensed to give a change in electron count for an atom or GB. Condensed Fukui functions for the removal of an electron are calculated as

$$f_\omega^- = \int_{\omega(N)} \rho(\mathbf{r}, N)\, d\tau - \int_{\omega(N-1)} \rho(\mathbf{r}, N-1)\, d\tau \tag{2}$$

and for the addition of an electron as

$$f_\omega^+ = \int_{\omega(N+1)} \rho(\mathbf{r}, N+1)\, d\tau - \int_{\omega(N)} \rho(\mathbf{r}, N)\, d\tau \tag{3}$$

where ω indicates an atomic basin, GB, or other region. Note that the region most likely to undergo electrophilic or nucleophilic attack in a molecule will have the largest positive value for eq 2 or 3, respectively.

CDFT has recently been extended to include the effect of EFs as well as other external factors.[19,44] The most relevant first- and second-order response functions including electric fields, $\boldsymbol{\varepsilon}$, are

$$\boldsymbol{\mu}^{\mathrm{dip}} = \left(\frac{\partial E}{\partial \boldsymbol{\varepsilon}}\right)_{N,v(\mathbf{r})} \tag{4}$$

$$\mathbf{A} = \left(\frac{\partial^2 E}{\partial \boldsymbol{\varepsilon}^2}\right)_{N,v(\mathbf{r})} \tag{5}$$

$$\left(\frac{\partial \rho(\mathbf{r})}{\partial \varepsilon}\right) = \left(\frac{\partial^2 E}{\partial \varepsilon \delta v(\mathbf{r})}\right)_N \tag{6}$$

where $\boldsymbol{\mu}^{\mathrm{dip}}$ is the dipole vector and $\mathbf{A}$ is the polarizability tensor. The quantity given by eq 6 is referred to as the EF-induced density and will be discussed in detail in this work. In eq 6, the vector character of $\boldsymbol{\varepsilon}$ is no longer considered, as the fields used in this work are homogeneous and oriented along a Cartesian axis; thus, ε is the value of the corresponding component of the EF.

Fukui functions can also be calculated for systems in EFs.[19] For the addition of an electron, this is calculated as

$$f^+(\mathbf{r};\, a) = \rho_{N+1}(\mathbf{r};\, \varepsilon = a) - \rho_N(\mathbf{r};\, \varepsilon = a) \tag{7}$$

where a is is the strength of the EF. Note that eq 7 considers how $\rho(\mathbf{r})$ will rearrange due to the addition of an electron where both the neutral and charged molecule are perturbed by

https://doi.org/10.1021/acs.jpca.3c01757
J. Phys. Chem. A 2023, 127, 4682−4694

the EF. In this work, however, we consider how $\rho(\mathbf{r})$ is redistributed due to an EF rather than from a change in overall electron count.

Molecules Studied. The set of molecules studied in this work include H_2, N_2, O_2, F_2, Cl_2, HF, HCl, CO, CO_2, and HCN. This set of molecules was chosen based on the fact that they all have at least $C_{\infty v}$ symmetry and include a variety of bond types as well as magnitudes of dipoles and polarizabilities, as shown in Table 1. As mentioned above, molecules

Table 1. Dipole Moment Magnitudes, Polarizabilities, Bond Lengths, and Bond Energies (BEs) with no EF for the set of molecules studied

molecule	dipole moment (D)[a]	polarizability (Å^3)[a]	bond length (Å)[b]	BE (kcal/mol)[b]
H_2	0	0.787	0.7386	−211.16
N_2	0	1.710	1.0862	−600.06
O_2	0	1.562	1.1921	−452.52
F_2	0	1.160	1.3678	−247.57
Cl_2	0	4.610	1.9902	−181.97
HF	1.827	0.800	0.9205	−297.44
HCl	1.093	2.515	1.2787	−218.20
CO	0.112	1.953	1.1204	−535.21
CO_2	0	2.507	1.1549	−830.90
HCN	2.980	2.593	1.0663,[c] 1.1415[d]	−660.41

[a]Experimental values from NIST.[46] [b]Theoretical values from this work. [c]H−CN. [d]HC−N.

with $C_{\infty v}$ (or $D_{\infty v}$) symmetry can be analyzed using rotational GBs. This method creates 1D plots of data which can be interpreted more easily than triangulated GB data from less symmetric systems. Even when an electric field is applied along the bond axis, $C_{\infty v}$ symmetry is maintained. The molecular set includes single, double, and triple bonds with a large range of bond strengths. Bond energies (BEs) are calculated as the difference in energy of the entire compound and its individual isolated atoms.[45] For example, the bond energy for CO_2 is calculated as

$$\mathrm{BE} = E(\mathrm{CO_2}) - [E(\mathrm{C}) + 2E(\mathrm{O})] \tag{8}$$

The dipole moment magnitudes range from zero to 2.980 D (HCN), and the polarizabilities range from 0.787 Å^3 (H_2) to 4.610 Å^3 (Cl_2).

This set expands on the pioneering work by Clarys et al. studying eqs 4−6 primarily for dihalogens subjected to EFs.[19] In their work, they focused on trends related to polarizabilities and hence studied nonpolar molecules. We now investigate the EF-induced density of molecules with permanent dipole moments.

Computational Details. All calculations were performed with the Amsterdam Density Functional package within the Amsterdam Modeling Suite.[45,47] The M06-2X functional was used for all reported results, as it performs well for dispersion-dominated systems.[48,49] Since DFT methods are known to not always be accurate for polarizability,[50] we tested CCSD methods for carbon monoxide and obtained qualitatively the same results as those shown in Figure 4 using M06-2X. We plan to perform a more in-depth systematic study comparing EF-induced densities from various calculation methods in the future. A nonrelativistic augmented triple-ζ double polarized basis set[51] with no frozen core was used to properly account for the redistribution of $\rho(\mathbf{r})$ from the added EFs, as has been done in other works.[19,52−54] All calculations were restricted except for O_2, which was unrestricted in a triplet state. Calculations were performed with a Becke 4 numerical integration quality (estimated bonding energy accuracy ΔE of <0.0005 mHartree),[55] default convergence tolerance, and QTAIM analysis with 0.1 Å spacing in the grid searching for critical points.[56,57] All reported atomic charges are QTAIM (Bader) charges.

Optimized geometries were obtained for the unperturbed systems aligned to the z axis with symmetry enforced. We define atom 1 as the atom at the origin and atom 2 (and atom 3, when applicable) in the $+z$ direction. Subsequent constrained nuclear position (CNP) and geometry optimization (GO) calculations were performed with a 1.0 V/Å EF (approximately 0.02 au) applied as a perturbation to the Fock operator. Other works have found this EF strength to be appropriate for modeling effects on small molecules, as it is on the high end of the EF strengths observed in enzyme active sites and what can be achieved experimentally in STM experiments.[19,21,22] EFs are discussed following the physicist convention of negative charge terminating at positive charge. For parallel and antiparallel EFs, rather than applying EFs in the positive and negative z direction, we chose to change the molecule orientation and always apply $+z$-direction EFs, as shown in Figure 1. We then discuss the effect of EFs on

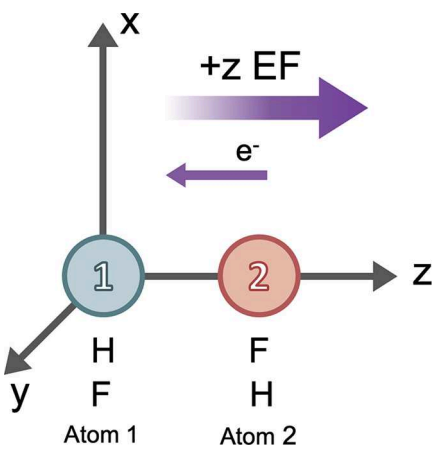

Figure 1. EFs are applied in the $+z$ and $+x$ directions in this work, which generally redistribute electrons in the $-z$ and $-x$ directions, respectively. All molecules are initially aligned on the z axis with atom 1 at the origin and additional atoms in the $+z$ direction. Heteronuclear molecules are subjected to $+z$-direction EFs using both possible molecular orientations, as shown for HF and FH.

heteronuclear molecules in terms of which atom is at the origin, *e.g.*, HF (atom 1 = H) and FH (atom 1 = F), rather than a $+z$- and $-z$-direction EF acting on HF.

For GB analysis, cube files of $\rho(\mathbf{r})$ data were created with 0.003 Å grid spacing and imported to Tecplot[58] using the Bondalyzer add-on package.[59] Thirty-six GBs for each atom were constructed in Tecplot from gradient paths seeded 0.1 Å from each atom's nucleus with equal spacing, as has been done in other works.[34,37−39] GBs were cut off at $\rho(\mathbf{r}) = 10^{-4}$ e/Å^3. Electron integrations were performed with the second-order trapezoidal method in Tecplot. All gradient paths were reseeded in the systems perturbed by an EF resulting in differences according to the response of a molecular fragment

https://doi.org/10.1021/acs.jpca.3c01757
J. Phys. Chem. A 2023, 127, 4682−4694

(RMF) method,[60−62] as has been done in other works calculating GB-condensed Fukui functions.[39,40]

RESULTS AND DISCUSSION

Bond energies from full geometry optimization calculations of molecules subjected to parallel and perpendicular EFs are first compared to results of calculations with various levels of geometry constraints. GB analysis is then performed on EF-induced densities from CNP calculations. Finally, the GB-condensed EF-induced densities are compared to expected regions of electron gain and loss using frontier molecular orbital (FMO) theory.

Effect of Fixed External Potential on EF-Induced Density. While the CDFT definition of induced density, eq 6, requires a fixed external potential (CNP calculation), one can also observe the change in $\rho(\mathbf{r})$ due to an EF when the nuclei are allowed to move (GO calculation). If the bond energies from these different calculations are similar, one can then apply results from EF-induced density calculations to situations where nuclei are free to move. Experimentally, there are some instances where nuclei can move freely, such as in gas-phase or solution reactions. However, there are also times when the motion of nuclei is at least somewhat restricted, such as in the solid phase or in the active sites of enzymes. To explore these differences, calculations with 1 V/Å parallel (along z axis) and perpendicular (along x axis) EFs were performed on the set of 10 linear molecules. All bonds were initially positioned along the z axis as shown in Figure 1. Four types of calculations were performed: (1) full geometry optimization (GO), (2) constrained bond length (CBL), (3) constrained angles (CA), and (4) constrained nuclear positions (CNP). The changes in bond energies and bond lengths were determined for each calculation, where bond energy values encompass all bonds in a molecule using eq 8 rather than considering individual bonding interactions.

Bond Energy. It is known that EFs applied to homonuclear diatomic molecules always lower the energy of the system. Heteronuclear molecules can be stabilized or destabilized by an EF depending on the direction in which it is applied.[22] The change in energy of a molecule due to a homogeneous EF can be approximated with the power series[63,64]

$$\Delta E \equiv E(\boldsymbol{\varepsilon}) - E(0) = -\mu^{\mathrm{dip}}\varepsilon\cos\theta - \frac{1}{2}\alpha_{\parallel}\varepsilon^2\cos^2\theta - \alpha_{\perp}\varepsilon^2\sin^2\theta + \cdots \quad (9)$$

where ε is the magnitude of the EF, μ^{dip} is the magnitude of the dipole moment of the unperturbed (no EF) molecule, $\alpha_{\parallel}$ and $\alpha_{\perp}$ are the parallel and perpendicular components of the unperturbed polarizability tensor, respectively, as given by eqs 4 and 5, and θ is the angle between the dipole moment vector and the direction of the homogeneous EF.

Figure 2 shows the percent change in bond energy due to a 1 V/Å perpendicular EF. Performing a full GO resulted in the largest change in bond energy for all molecules since each molecule could alter its bond lengths and rotate to align with the EF. Constraining the bond length gave almost identical results to the geometry optimization. In this case, molecules were still allowed to rotate in order to align with the EF along the x axis. Alternatively, constraining the molecule along the z axis did not result in as large of a stabilizing effect from the EF as observed when rotation was allowed. This difference in

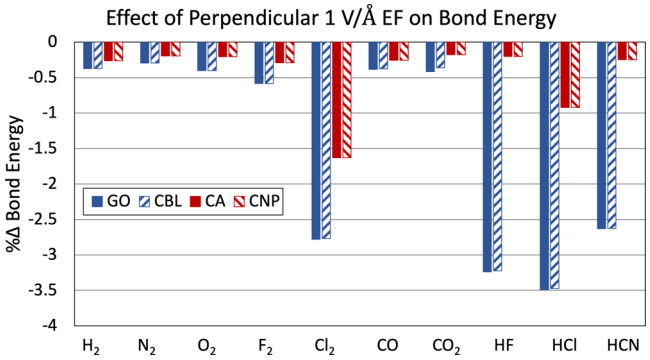

Figure 2. Changes in bond energy from a perpendicular 1 V/Å EF with various levels of geometry optimization: (1) full geometry optimization (GO); (2) constrained bond length (CBL); (3) constrained angles (CA); (4) constrained nuclear positions (CNP).

stabilization was greater for polar molecules than for molecules with no permanent dipole moment or a small dipole moment (CO), as can be seen in eq 9.

When a molecule is allowed to rotate and align with an EF, the change in energy can be approximated as

$$\Delta E \approx -\mu^{\mathrm{dip}}\varepsilon - \frac{1}{2}\alpha_{\parallel}\varepsilon^2 \quad (10)$$

since $\theta = 0$. When rotation is not permitted, a perpendicular EF causes the change in energy approximated by

$$\Delta E \approx -\alpha_{\perp}\varepsilon^2 \quad (11)$$

as $\theta = \pi/2$. Thus, the dipole moment has a strong effect on the energy of a molecule in a parallel field (or perpendicular field that a molecule is allowed to align with by rotation) according to eq 10 but should not affect the energy of a molecule in a perpendicular field if rotation is not allowed, as shown in eq 11.

Whether or not the bond length was allowed to change along with the rotation had a negligible effect on the change in bond energy, with the slight exception of CO_2, which had a difference of 0.44 kcal/mol between the GO and CBL calculations due to the large change in bond lengths seen in this molecule from an applied EF. The uniqueness of CO_2 in this regard is discussed in more detail below. For an EF to have the largest energetic effect on a molecule, the molecule must be allowed to rotate, but changing bond length is generally insignificant. While molecules are able to rotate to align with EFs in the gas phase, this rotation is often prohibited by steric considerations such as in enzymes. However, molecular rotation is far more important than changes in bond lengths for stabilization of molecules in an EF. This is in line with the idea proposed by Wang et al. of using oriented external EFs as catalytic tweezers to position molecules in space to lower activation barriers.[65]

For parallel EFs applied to linear molecules, CNP calculations can be used in place of GO calculations with minimal differences in bond energies, as demonstrated in Figure 2. The important exception here is for highly polar heteronuclear molecules such as HCN. In this case, a CNP calculation would not capture realistic changes in energy for a $+z$-direction EF, as this direction of EF caused the HCN molecule to rotate 180° to align its dipole moment with the EF. An optimization of HCN that does not allow for rotation with a $+z$-direction EF had a 1.8% change in bond energy, while a $-z$-direction EF incurred a −2.6% change in bond

https://doi.org/10.1021/acs.jpca.3c01757
J. Phys. Chem. A 2023, 127, 4682−4694

energy. This discrepancy is not shown in Figure 2 since a perpendicular field was used rather than a $\pm z$-direction EF (see Table S1 for parallel/antiparallel EF data). For CO, the dipole moment is of a small enough magnitude that the dipole switched direction rather than the molecule rotating when a $-z$-direction EF was added to the system and a full GO was performed.

Bond Length. Figure 3 shows the percent change in bond lengths due to a 1 V/Å parallel or perpendicular EF when

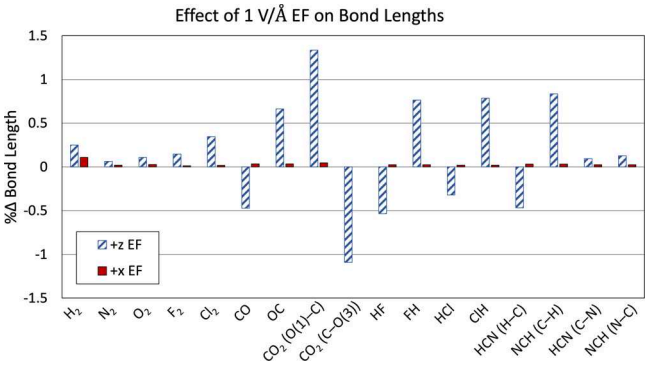

Figure 3. Percent changes in bond length due to parallel (z-direction) and perpendicular (x-direction) 1 V/Å EF. No rotation of the molecules was allowed. Note that for $C_{\infty v}$ molecules, the z-direction EF was applied for both orientations of the molecule along the z axis.

rotation of the molecules was not allowed. For molecules with only $C_{\infty v}$ symmetry, the z-direction EF was applied for both orientations of the molecule along the z axis. Also note that the x-direction EF gave identical results for both orientations. Bond lengths for all molecules changed significantly more for the parallel EFs compared to the perpendicular EFs, as has been noted in other work.[19] The small changes in bond lengths for these systems (<1% for most molecules) support the energetic data showing that allowing bond lengths to change does not have a significant effect on bond energies. Previous work has demonstrated that bond lengths change quadratically with the strength of EF.[19,22] Since a relatively large EF strength (1 V/Å) was used in this work, most experimental bond length changes due to EFs will be even smaller than the data shown in Figure 3.

The most significant changes in bond lengths occurred in CO_2, with changes greater than 1% for the z-direction EF. The next largest changes all involved hydrogen atoms (FH, ClH, and NCH). None of the homonuclear diatomic molecules had significant changes in bond length when the 1 V/Å EF was applied. For the remainder of this paper we show only results from EFs in the z direction to maintain $C_{\infty v}$ symmetry. Additionally, after an initial test of GB analysis performed on GO and CNP calculations, we only present data from CNP calculations, as EFs have a minor effect on bond length and this small change in bond length subsequently plays a minor role in bond energies.

Gradient-Bundle-Condensed EF-Induced Densities. GB analysis was performed on molecules subjected to parallel 1 V/Å EFs in order to quantify the redistribution of $\rho(\mathbf{r})$ within atomic basins.

Overview of Data Interpretation. To more easily interpret the changes in GBs due to EFs, simplified 1D representations were created to show the relative percent changes in electron counts. An example of these data for carbon moxide is shown in Figure 4. The GB image in Figure 4a shows the shape and size of a cutplane of the 36 GBs created in each atomic basin. The GBs are colored to show where loss of electrons (red) and gain of electrons (blue) occur. Each of these electron changes is quantified as a percent change in electron count according to

$$\%\Delta N = 100\left(\frac{N_{\mathrm{EF}} - N_{\mathrm{NoEF}}}{N_{\mathrm{NoEF}}}\right) \tag{12}$$

where N_{EF} and N_{NoEF} give the electron counts in each GB with an EF or no EF, respectively. A percent change in electron count is used to account for the fact that GBs can have drastically different sizes even when the gradient paths defining each GB are seeded with equal spacing. For example, GB36 in the carbon atom of CO is significantly larger than GB1 of the carbon atom, as shown in Figure 4a.

For diatomic molecules, GBs are numbered starting with GB1 along the bond/interatomic surface (IAS) and moving out from the IAS for each atom until GB36 is reached. GB1 is thus always along the bond/IAS for diatomic molecules. For triatomic molecules, GBs are simply numbered from left to right, such that GB1−GB36 are in atom 1, GB37−GB72 are in atom 2, and GB73−GB108 are in atom 3. Figure 4b shows the $\%\Delta N$ in each GB, which is then converted to a simplified 1D representation of the data in Figure 4c for ease of comparing the GB-condensed EF-induced densities across molecules. The darkness of the color for each GB is linearly scaled with $\%\Delta N$, and the darkest color is determined internally to each atom using the largest value of $|\%\Delta N|$. For less symmetric $C_{\infty v}$ molecules, both orientations of the molecule along the z axis are included, where the EF always points from atom 1 (left) to atom 2 (right). Figure 5 shows simplified 1D representations of the $\%\Delta N$ in all molecules studied in this work. Plots of $\%\Delta N$ for all molecules are shown in Figures S1−S14.

Comparison of GO and CNP EF-Induced Densities. GB-condensed EF-induced densities were initially calculated for both GO and CNP calculations to ensure that there were not large discrepancies in the data between these two calculation methods (simplified 1D representations of GO results are shown in Figure S15). As expected from the results in Figures 2 and 3, whether or not bond lengths were allowed to change did not have a large effect on the EF-induced densities, with the exception of CO_2. Results for F_2, Cl_2, HF, HCl, CO, and HCN were essentially identical for the two calculation methods, and slight differences occurred for H_2, N_2, and O_2. For these three molecules, the differences in GB-condensed EF-induced densities occurred in GB1 of either atom 1 (H_2 and O_2) or atom 2 (N_2), meaning discrepancies along the bond and IAS. GB1 in H_2 had a slight decrease in electron count in atom 1 when the bond length was allowed to change but a slight increase when the nuclear coordinates were fixed. Similarly, O_2 had a greater decrease in atom 1 GB1 for the GO calculation than in the CNP calculation. For N_2, atom 2 GB1 had a slight decrease for the GO calculation and slight increase for the CNP calculation.

In CO_2, the discrepancies between GO and CNP calculations occurred in the carbon atomic basin. For the GO, the carbon basin gained electrons near O(1) in GB37−GB40 and lost electrons near O(3) in GB70−GB72. The opposite behavior is shown in the EF-induced density for the CO_2 CNP calculation. Here the GBs near O(1) lost electrons and the GBs near O(3) gained electrons. This behavior in CO_2 can be rationalized by the change in the C−O bond lengths

https://doi.org/10.1021/acs.jpca.3c01757
J. Phys. Chem. A 2023, 127, 4682−4694

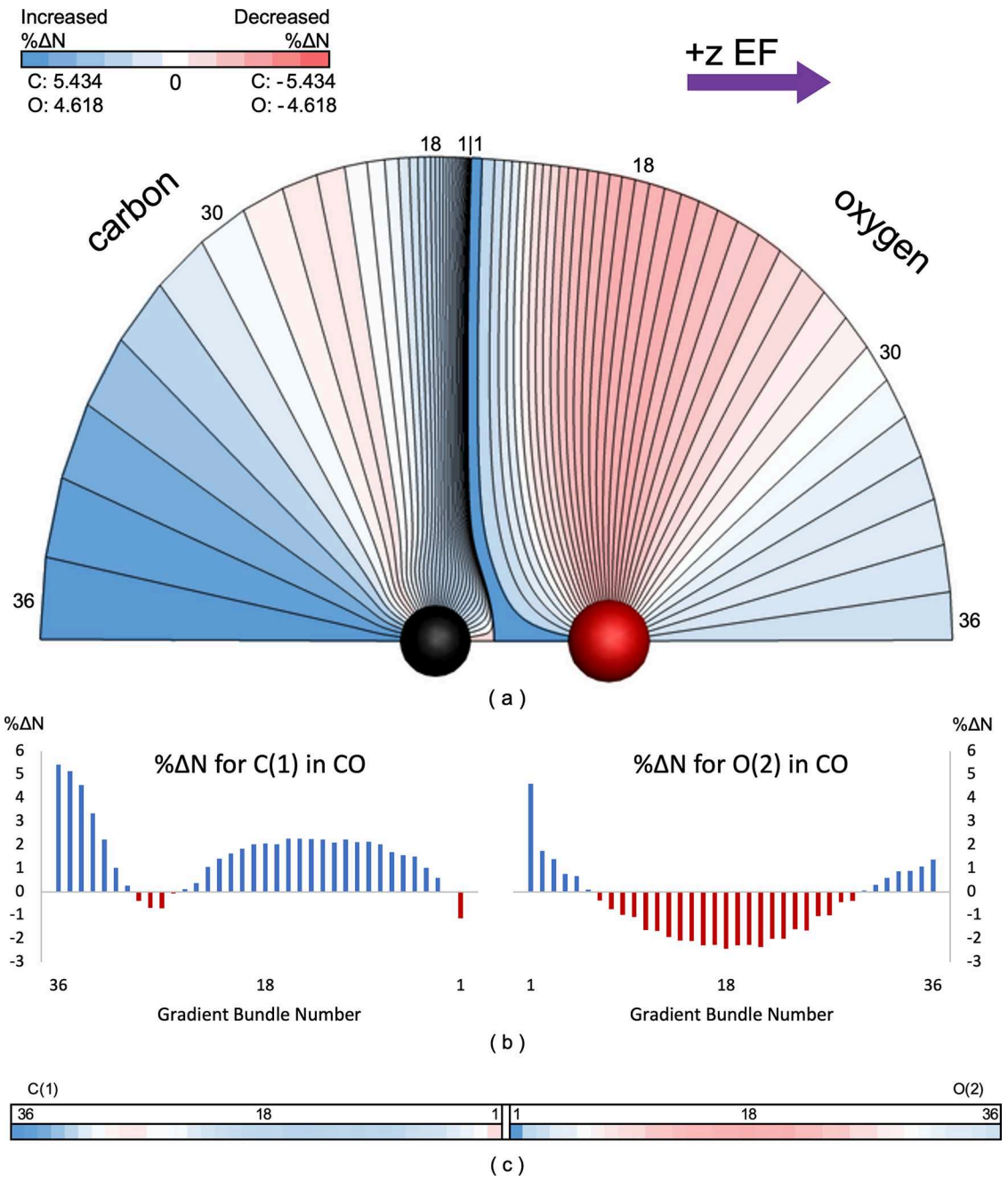

Figure 4. GB-condensed induced densities from +*z*-direction 1 V/Å EF applied along the bond axis for CO. (a) Sizes and shapes of the GBs with no EF, colored to match the %Δ*N* due to the EF. (b) Plots of the %Δ*N* in each of the 36 GBs around each atom from the EF. (c) Simplified 1D representation of the EF-induced density for each GB. Blue indicates an increase in electron count, and red indicates a decrease in electron count in all figures.

due to an EF and the size of the carbon atomic basin. As shown in Figure 3, the C−O(1) bond length increased by 1.3% and the C−O(3) bond length decreased by 1.1% from a 1 V/Å EF in the +*z* direction. Considering all the other molecules in this study, the next largest changes in bond lengths were an increase of 0.8% in the C−H bond of NCH and a decrease of 0.5% in HF. Substantial changes in bond lengths were required in CO_2 for the molecule to be most stabilized by an EF. This may be partially due to the small size of the carbon atomic basin in CO_2 (30.9 au with a cutoff of $\rho(\mathbf{r}) = 10^{-3}$ e/Å^3 compared to the carbon atoms in CO and HCN having volumes of 111.6 and 87.4 au, respectively).

Since allowing the bond length to change when a molecule is perturbed by an EF generally plays an insignificant role in how $\rho(\mathbf{r})$ is rearranged, we only include CNP calculations moving forward, which corresponds to the CDFT EF-induced density definition given by eq 6. Whether or not the nuclei are allowed to move when a linear molecule is subjected to a 1 V/Å parallel EF gives essentially the same results for the EF-induced density of molecules tested here, with the exception of CO_2.

General Trends in EF-Induced Density. While significant rearrangement of $\rho(\mathbf{r})$ within atomic basins did occur for all molecules tested, few consistent trends were found between the GB-condensed EF-induced density of molecules included in this study and bond strength, bond length, polarity, and

https://doi.org/10.1021/acs.jpca.3c01757
J. Phys. Chem. A 2023, 127, 4682−4694

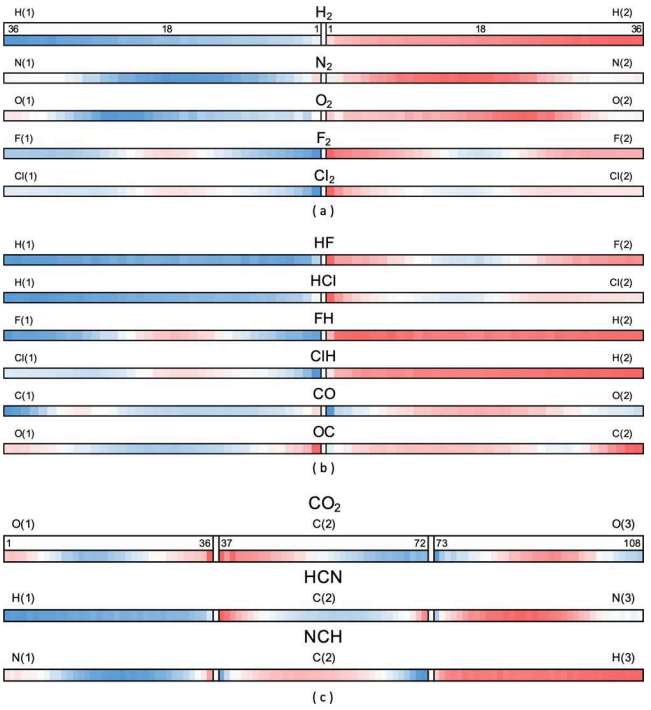

Figure 5. Relative changes in electron counts of gradient bundles for molecules subjected to +z-direction 1 V/Å EF. (a) Homonuclear diatomic molecules and (b) heteronuclear diatomic molecules have GB1 (along bond path/IAS) in the center of each image, and GB36 is seeded 180° away from the bond path for each atom. (c) Triatomic molecules have the 36 GBs in each atomic basin numbered from left to right such that GB1−GB36 are in atom 1, GB37−72 are in atom 2, and GB73−108 are in atom 3.

polarizability. However, more trends were discovered with the diatomic molecules than the triatomic molecules, and these molecules will thus be focused on in this section. Despite the fact that an EF in the +z direction should increase the amount of $\rho(\mathbf{r})$ in atom 1 and decrease the amount of $\rho(\mathbf{r})$ in atom 2 for diatomic molecules, most atoms in the molecules tested here had some "unexpected" electron gain (atom 2) and loss (atom 1) as well.

For all of the molecules tested, hydrogen is the only atom with no unexpected gain or loss in its EF-induced density, even in the triatomic HCN molecule. The greatest %ΔN occurred in the larger-numbered GBs away from the bonding region. For most other atoms, the largest %ΔN occurred closer to the bonds and IASs. The other exceptions were the fluorine atom in FH, which had a similarly large %ΔN in GBs near the bond and 180° away from the bond, and the carbon atom in CO and OC, which also had the largest change 180° from the bond.

In all of the homonuclear diatomic molecules shown in Figure 5 other than H_2, there was unexpected loss/gain of electrons in various GBs. For N_2 the only significant unexpected loss or gain occurred in GB1 of both atoms. For O_2, there was slight unexpected loss and gain in the GBs furthest from the bond. For the dihalogens, unexpected gain and loss occurred in the GBs centered around GB18. Considering the entire molecular set, all of the molecules with unexpected loss in GB1 of atom 1 (or 2) also had unexpected gain in GB1 of atom 2 (or 3) and occurred in triple bonds (N_2, CO, and OC, CN in HCN, and NC in NCH). There seems to be a compensating effect along the bond paths and IASs for these molecules.

Most atoms gained/lost electrons in similar regions regardless of whether they were atom 1 or atom 2 (or atom 3 for triatomics). For example, atom 1 in F_2 had unexpected loss in GB15−GB21, and atom 2 had unexpected gain in GB15−GB21. Considering a triatomic molecule, O(1) in CO_2 lost electrons in GB1−GB8 and GB31−36 while gaining electrons in the central GBs. O(3) had the opposite behavior, as it gained electrons in GB73−GB80 and GB104−GB108 and lost electrons in the central GBs. The amounts of electrons gained/lost were also similar, as shown in Table S2. These results were unexpected, as electron gain/loss often corresponds to locations of HOMO and LUMO lobes, which are generally not identical. We explore the relationship between frontier molecular orbitals (FMOs) and electron loss/gain due to an EF in more detail in the following section.

Additionally, GB behavior within each atom varied depending on which molecule the atom was part of in most cases. Consider that O(2) in O_2 only gained electrons in the GBs away from the bond while the O in CO gained electrons in GB1−GB5 as well as in GB32−GB36. The O in OC lost electrons in GB1−GB4 and GB31−GB36. Considering the triatomics, O(3) in CO_2 gained electrons in GB73−GB81 (near the O(1)−C bond) and GB103−GB108 (pointing away from the C−O(3) bond). A similar pattern of electron loss occurred in O(1) of CO_2. Thus, the GB-condensed EF-induced density of atoms does not appear to be transferable between all molecules. The exception here was for halogen

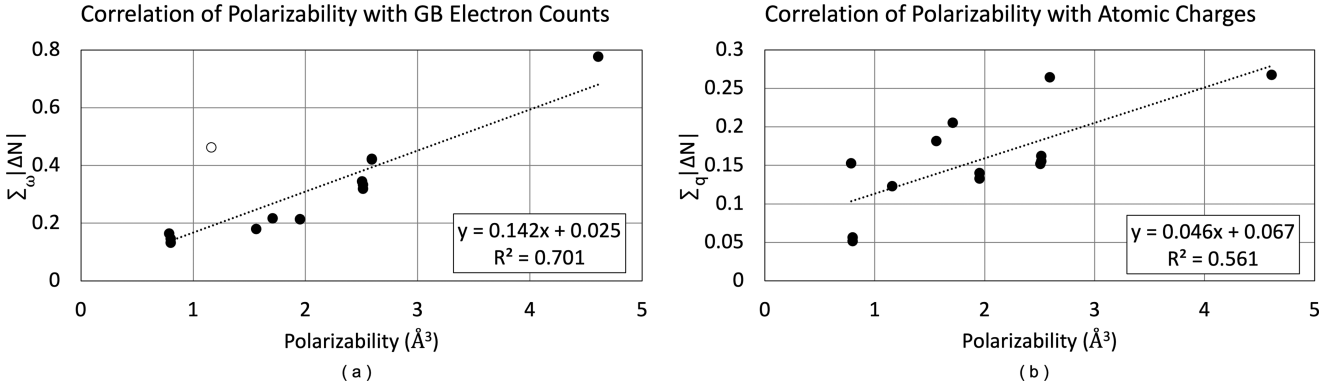

Figure 6. Correlation of experimental polarizabilities of molecules[46] with the sum of absolute values of changes in electron counts due to a 1 V/Å parallel EF. (a) Changes in electron counts for each GB. (b) Changes in electron counts for each atomic basin. F_2 is a clear outlier for GB correlation and is shown as an open circle but still included in the linear regression.

https://doi.org/10.1021/acs.jpca.3c01757
J. Phys. Chem. A 2023, 127, 4682−4694

atoms. Whether a halogen atom (X) is in a HX or X_2 molecule did not generally change the regions of GBs that gained or lost electrons. While few consistent trends were found between regions of electron gain/loss and the molecular properties in Table 1, the next section considers how these regions correspond to FMOs.

Rather than considering the specific GBs that lose or gain electrons due to an EF, one can also observe the absolute value of the change in the number of electrons in all GBs of an atom, $\sum_\omega|\Delta N|$, where ω indicates a GB. Here there was a clear correlation with polarizability of molecules as shown in Figure 6a, as expected since polarizability can be interpreted as how easily $\rho(\mathbf{r})$ can be rearranged. The outlier in this trend was F_2, which had a larger rearrangement of $\rho(\mathbf{r})$ than expected from its experimental polarizability. If F_2 is removed from the data, the R^2 value increases from 0.701 to 0.912.

Interestingly, the correlation of polarizability with the absolute changes in atomic charges, q, due to EFs using QTAIM shown in Figure 6b is not as strong as when the changes in each GB were considered in Figure 6a. Despite some atoms having small changes in atomic charge, there was often still a large rearrangement of $\rho(\mathbf{r})$ *within* the atomic basin. The most striking examples of this occurred in molecules with halogen atoms. For example, Cl_2 had $\sum_\omega|\Delta N| = 0.78$ but $\sum_q|\Delta N| = 0.27$. HF had $\sum_\omega|\Delta N| = 0.15$ but $\sum_q|\Delta N| = 0.06$. This is a clear example of where condensing properties over atomic basins does not provide an accurate picture of how molecules respond to perturbations. A finer partitioning of space is required to capture the full redistribution of $\rho(\mathbf{r})$ due to an EF.

Relationship to Frontier Molecular Orbitals. Here we determine whether regions of electron loss and gain due to an EF correspond to the frontier molecular orbitals (FMOs) in molecules, as one might expect. Previous work with GB analysis investigated the rearrangement of $\rho(\mathbf{r})$ with GB-condensed Fukui functions.[39] The change in electron count of each GB was compared for a system's unperturbed $\rho(\mathbf{r})$ to the $\rho(\mathbf{r})$ of the same system with an electron removed or added. A key finding from this work was that electron count differences in GBs correlated to regions where FMO lobes existed, corresponding to regions most likely to undergo nucleophilic or electrophilic attack. When an electron was removed from the system, the GBs experiencing a decrease in $\rho(\mathbf{r})$ spatially aligned with the neutral system's HOMO. When an electron was added to the system, the GBs experiencing an increase in $\rho(\mathbf{r})$ spatially aligned with the neutral system's LUMO. Additionally, GBs with negative Fukui functions, regions with "unexpected" electron gain/loss, occurred where FMO nodes existed, as anticipated from work studying (noncondensed) Fukui functions.[66−68]

In the case of an applied +z-direction EF, no electrons are removed from or added to the molecular system, but $\rho(\mathbf{r})$ is rearranged such that there is an expectation for atom 1 to generally gain electrons and atom 2 to generally lose electrons. Therefore, one might hypothesize that GBs with a loss of electrons in atom 2 due to the EF would correspond to loss of $\rho(\mathbf{r})$ from the HOMO. Similarly, addition of electrons to GBs in atom 1 due to the EF would correspond to the lobes of the LUMO, which gain $\rho(\mathbf{r})$. However, our results indicate that $\rho(\mathbf{r})$ rearrangement due to an EF is quite different from rearrangement caused by adding or removing an electron. It is worthwhile to note that although the previous work[39] observed strong agreement between GB changes and the shapes of FMOs with Fukui functions, GBs and orbitals are intrinsically different volumes. Molecular orbitals are often displayed with isosurfaces of $\rho(\mathbf{r})$, while GBs are created with ZFSs in $\nabla\rho(\mathbf{r})$. It is thus unlikely to ever have perfect spatial alignment between orbitals and GBs.

For diatomic molecules, there was little to no spatial alignment between electron loss in atom 2 GBs and the lobes of the unperturbed molecule's HOMO. The only systems which appeared to correlate for electron loss were H_2 and O_2. As shown in Figure 7b, the GBs in O_2 atom 2 which lost

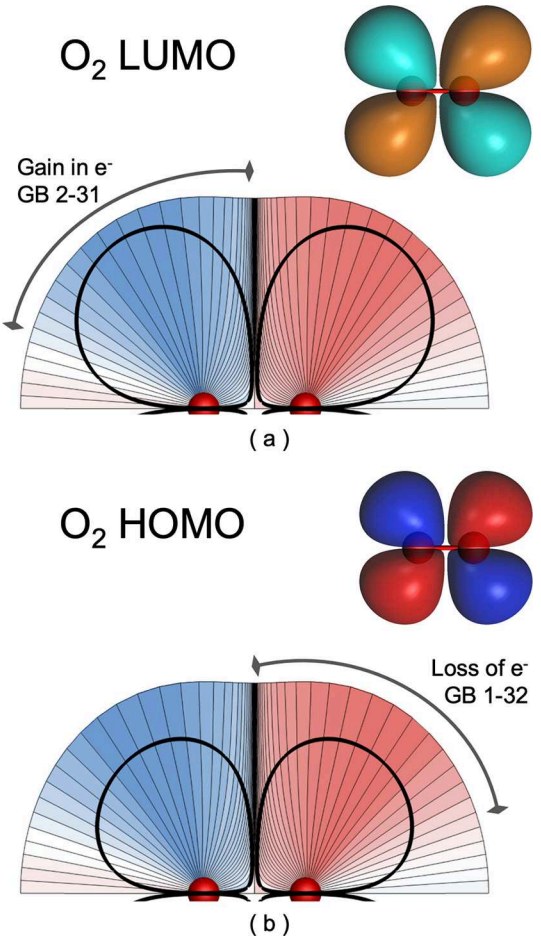

Figure 7. Overlay of O_2 GBs with the (a) LUMO (isosurface = 0.03 au) and (b) HOMO (isosurface = 0.03 au). Orbitals are from calculations with no EF. Each GB is colored according to its relative %ΔN due to +z-direction 1 V/Å EF.

electrons due to the EF spatially aligned with the π HOMO lobe. GBs in atom 2 with minimal change or slight increases in $\rho(\mathbf{r})$ corresponded to nodes. Similarly in Figure 7a, the atom 1 GBs which gained electrons aligned to the π LUMO while decreases in $\rho(\mathbf{r})$ occurred along nodes. Of the molecules studied, H_2 and O_2 are the only diatomic systems where expected spatial alignment existed for electron loss and gain with both the HOMO and LUMO lobes, respectively. However, note that H_2 and O_2 both have identically shaped HOMO and LUMO orbitals (see Figures S16−S21 for FMO overlays for additional molecules).

Other molecules, such as N_2 shown in Figure 8, gained electrons in atom 1 GBs that generally corresponded to the π LUMO but have no agreement for the loss of electrons in atom

https://doi.org/10.1021/acs.jpca.3c01757
J. Phys. Chem. A 2023, 127, 4682−4694

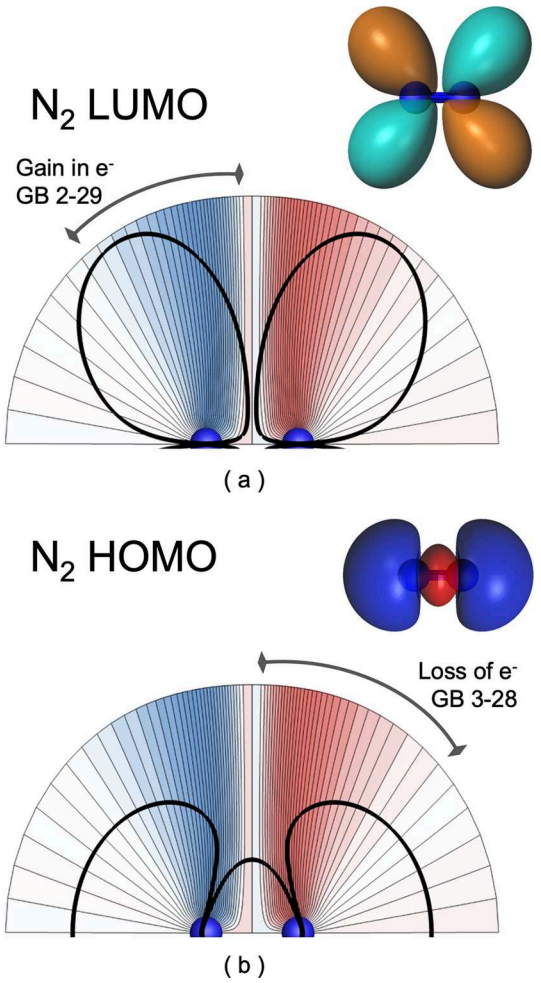

Figure 8. Overlay of N_2 GBs with the (a) LUMO (isosurface = 0.03 au) and (b) HOMO (isosurface = 0.03 au). Orbitals are from calculations with no EF. Each GB is colored according to its relative %Δ*N* due to the EF.

2 with the σ HOMO. Instead, the loss of electrons in atom 2 generally aligned to a node in the HOMO mirroring the gain of electrons in atom 1. Due to the symmetry of electron loss/gain, the GBs that lost electrons in atom 2 actually corresponded better with the LUMO than the HOMO.

All other diatomic molecules except CO presented similar patterns as N_2. There was generally consistency between electron gain in atom 1 GBs with the lobes of the unperturbed molecule's LUMO, but no spatial alignment of the loss of electrons in atom 2 GBs and the unperturbed HOMO. With an applied EF, there appeared to be a much stronger preference for LUMO lobes to gain electrons than for HOMO lobes to lose electrons. Interestingly, the loss of electrons in multiple molecules suggested general agreement with the shape of the LUMO. However, this may simply be due to the symmetry of electron loss and gain in each atom.

Since EFs allow for mixing of orbitals that was previously forbidden, it is possible that regions of electron loss/gain due to an EF better correspond with the product of filled and unfilled orbitals with the EF direction as given by

$$\langle \phi_1 | z | \phi_2 \rangle \tag{13}$$

where ϕ_1 and ϕ_2 could represent, for example, the unperturbed HOMO and LUMO, respectively. For the molecules tested here, the product of the HOMO and EF LUMO do not visually appear to spatially align with GB-condensed EF-induced densities, but it is possible that eq 13 would more accurately correspond to the induced density if orbitals other than the HOMO and LUMO were also considered.

The only diatomic molecule without any agreement for either the HOMO or LUMO was CO, as displayed in Figure 9. The GBs which lost electrons in atom 2 corresponded to a node in the σ HOMO, as shown in Figure 9c. Conversely, the

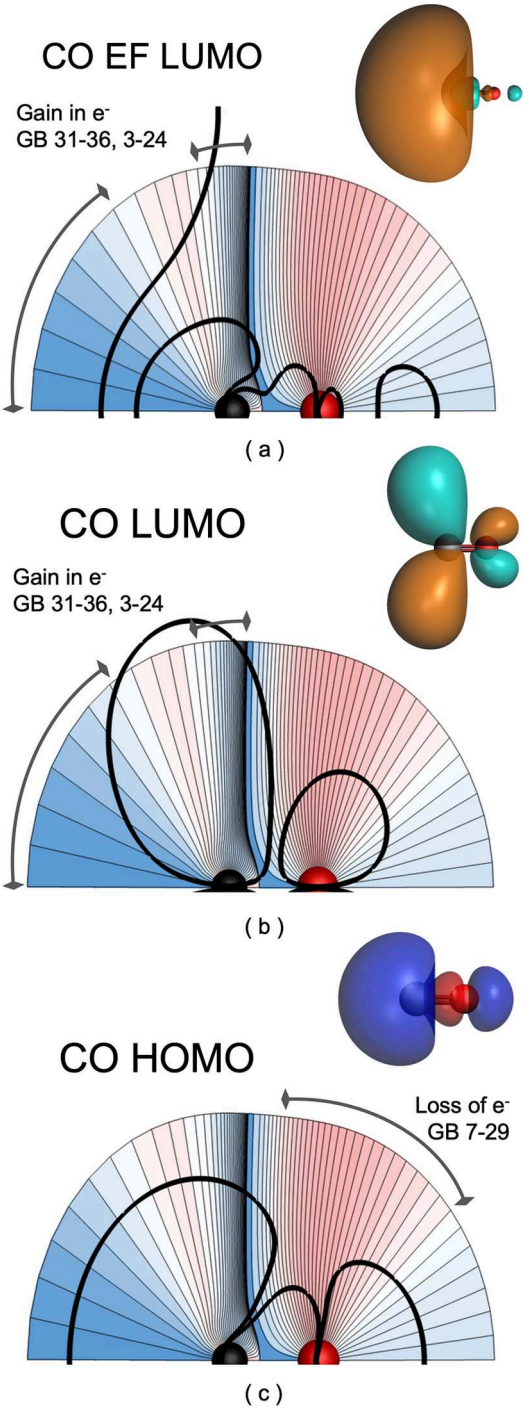

Figure 9. Overlay of CO GBs with the (a) +*z*-direction 1 V/Å EF LUMO (isosurface = 0.01 au), (b) no-EF LUMO (isosurface = 0.03 au), and (c) no-EF HOMO (isosurface = 0.03 au). Each GB is colored according to its relative %Δ*N* due to the EF.

https://doi.org/10.1021/acs.jpca.3c01757
J. Phys. Chem. A 2023, 127, 4682−4694

atom 1 GBs with the greatest gain in electrons shown in Figure 9b corresponded to a node in the unperturbed system's π LUMO. There are some GBs with electron gain spatially present in the π LUMO lobe, but there are GBs that lost electrons in this region also.

An additional point of consideration is that FMOs can become distorted in shape and change energy when an EF is applied to the molecule. None of the molecules tested here had any significant differences in their HOMO beyond the relative sizes of lobes changing. Size changes also occurred for the LUMOs, but three of the diatomic molecules, N_2, H_2, and CO, had completely different LUMOs with and without the EF due to energy changes. For example, the unperturbed CO molecule had two degenerate π LUMOs (only one is shown in Figure 9b) but its LUMO+1 was a σ orbital. When an EF was applied in the $+z$ direction, the π LUMO of the CO molecule remained relatively unchanged whereas the σ LUMO+1 drastically lowered in energy. This energy change caused the σ LUMO+1 to become lower in energy than the unperturbed π LUMO. Thus, the π LUMO and σ LUMO+1 switched places in the molecular energy diagram when a 1 V/Å EF was applied. Similar cases existed for N_2 and H_2, as shown in Figures S22–S24. The shape of the σ EF LUMO of CO is displayed in Figure 9a. However, this EF LUMO also did not have any obvious correlations with the atom 1 GB gains or losses.

The change in ordering of LUMOs due to EFs has been noted in other works[54,69−71] but to the best of our knowledge has not been studied in detail. We are currently investigating this phenomenon for the set of molecules studied here.

The analysis comparing FMOs and GB-condensed EF-induced densities of triatomic molecules was more challenging than for diatomics. Atom 1 was still expected to generally gain electrons, but atom 3 was expected to lose electrons while atom 2 could both lose and gain electrons. For CO_2, the HOMO aligned with GBs that lost electrons, as shown in Figure 10c. There was an increase of $\rho(\mathbf{r})$ along nodes and decreases of $\rho(\mathbf{r})$ that lined up with the HOMO lobe for atom 3. Analysis of atom 2 was challenging not only because of the competing loss and gain but also because the carbon atomic basin itself resided along a node in the HOMO. Furthermore, consideration of the LUMO was difficult because the donut-shaped σ LUMO does not spatially correspond well to any GB position. Similar to CO, the LUMO of CO_2 changed to a σ orbital when a 1 V/Å EF was applied as shown in Figure 10a. This EF LUMO still did not appear to have any obvious agreement to electron gain in O(1) or carbon GBs. For HCN and NCH, there was some agreement of the loss and gain of electrons with the LUMO and HOMO, but the size and overlap of the orbitals compared to the GBs themselves again hinder direct comparison.

Based on the molecule set tested here, there is rarely alignment of HOMO lobes with GBs that lose electrons. However, there is slightly better agreement with LUMO lobes and GBs that gain electrons. Overall, it appears that FMOs are not the driving factor for how EFs redistribute $\rho(\mathbf{r})$ within atomic basins, which is fundamentally different than results for GB-condensed Fukui functions. Additionally, LUMOs can drastically change energies due to EFs, causing a change in unoccupied FMOs. We are currently investigating whether the geometry of GBs is a better predictor of EF-induced density than FMOs, as the volumes of GBs and the curvature of their ZFSs have shown some correlation to EF-induced densities in a preliminary study.[40]

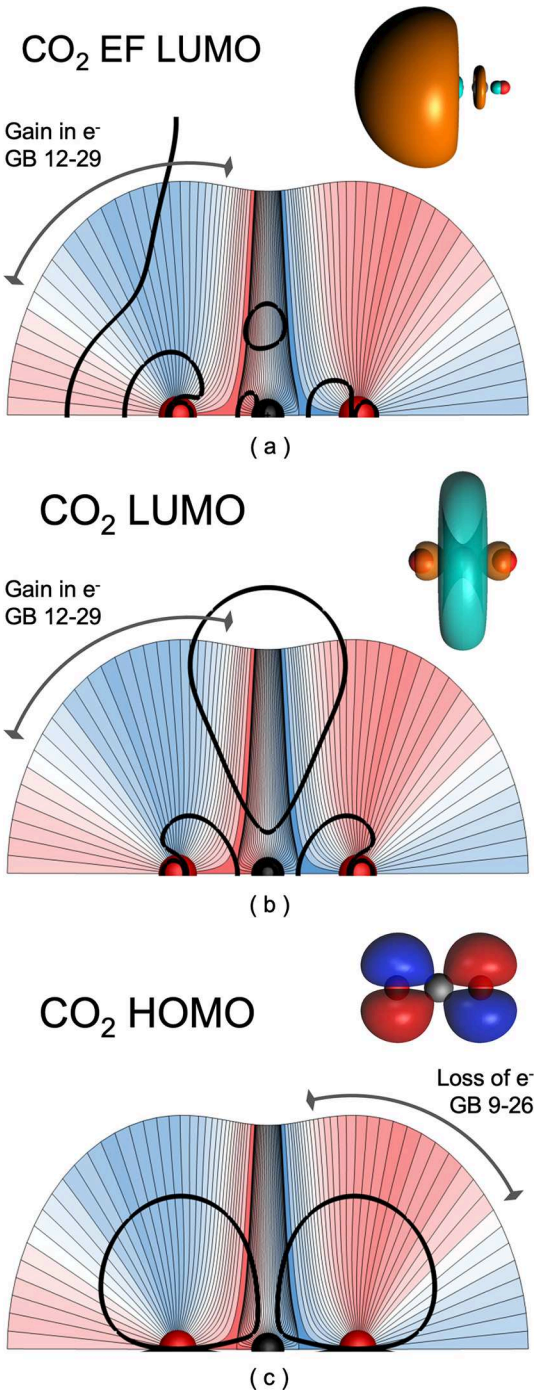

Figure 10. Overlay of CO_2 GBs with the (a) $+z$-direction 1 V/Å EF LUMO (isosurface = 0.015 au), (b) no-EF LUMO (isosurface = 0.03 au), and (c) no-EF HOMO (isosurface = 0.03 au). Each GB is colored according to its relative $\%\Delta N$ due to the EF.

CONCLUSIONS

This work studied the rearrangement of $\rho(\mathbf{r})$ in a set of diatomic and linear triatomic molecules when subjected to homogeneous EFs. We first demonstrated how allowing bond lengths to change when EFs are applied has a minimal impact on the resulting bond energies, in line with the small changes in bond lengths incurred by EFs. This validates using the CDFT-defined EF-induced density[19] to understand the effect of EFs on molecular systems whether or not the bond lengths of molecules are restricted such as in the active site of an

https://doi.org/10.1021/acs.jpca.3c01757
J. Phys. Chem. A 2023, 127, 4682−4694

enzyme. Rotation of molecules does have a significant effect on the energetic changes of molecules in external EFs.

To quantify the EF-induced density within atomic basins, we partitioned each atom into 36 gradient bundles bounded by ZFSs in $\nabla\rho(\mathbf{r})$. Few clear trends were found between the GB-condensed EF-induced density values and bond strength, bond length, polarity, or polarizability. All atoms except hydrogen had some regions of unexpected electron gain (in atoms that lost electrons overall) and unexpected electron loss (in atoms that gained electrons overall). The exact GBs where this unexpected loss and gain occurred varied from atom to atom and generally were not transferable between the same atom type in different molecules. We plan on expanding our original set of 10 molecules and studying the geometry of the charge density to determine why these unexpected regions of electron loss and gain occur in specific GBs.

We did find, however, that polarizability correlates better with changes in electron counts in GBs than it does with changes in atomic charges. Changes in atomic charges do not consider electron rearrangement within an atomic basin, only between basins. Since a large amount of unexpected electron loss/gain occurred in many atoms, changes in atomic charges therefore often drastically underestimate the total rearrangement of $\rho(\mathbf{r})$. Rearrangement of $\rho(\mathbf{r})$ within atomic basins must be considered to see the full effects of EFs on molecules, which we have shown can be accounted for using GBs.

Surprisingly, the regions of electron loss in the GBs of each atom did not correspond to the HOMO of most molecules, yet electron gain often aligned to the location of LUMO lobes. This is a drastically different picture than how $\rho(\mathbf{r})$ rearranges when electrons are gained/lost in a total molecule as shown by the Fukui function.[39] Apparently, the transfer of electrons between atoms and GBs within a molecule due to an EF is less influenced by molecular orbitals than the transfer of electrons during chemical reactions involving nucleophilic or electrophilic attack. However, unoccupied orbitals are often influenced by EFs, as the LUMOs of many molecules were shown to change when EFs were applied to the systems. While this has been noted in other works,[54,69−71] we are unaware of a systematic study of the phenomenon. Our preliminary results show that the strength of EF for which the crossing of the LUMO and LUMO+1 varies for each molecule, and this crossing is the focus of a current study.

The detailed study of the redistribution of $\rho(\mathbf{r})$ through GBs may provide insight on designing both external and internal EFs for catalysis. While defining a reaction axis along which to apply a homogeneous EF to control reactivity has been highly successful in many recent computational and experimental studies, it is not always straightforward to predict how an EF will affect a reaction, especially when heterogeneous EFs are considered. GB analysis thus allows for a high-resolution picture of electron rearrangement due to perturbations which may shed insight on how best to design EF-catalyzed reactions.

■ ASSOCIATED CONTENT

Supporting Information

The Supporting Information is available free of charge at https://pubs.acs.org/doi/10.1021/acs.jpca.3c01757.

Data for changes in bond energies due to ±z-direction EFs, plots of %ΔN due to EF for all molecules, 1D representations of %ΔN due to EF for GO calculations, table of total electrons gained and lost in all atoms due to EF, overlays of FMOs and GBs, and overlays of EF LUMOs with GBs (PDF)

■ AUTHOR INFORMATION

Corresponding Author

Amanda Morgenstern − *Department of Chemistry and Biochemistry, University of Colorado at Colorado Springs, Colorado Springs, Colorado 80918, United States;* orcid.org/0000-0001-9279-0588; Phone: 719-359-3449; Email: amorgens@uccs.edu

Authors

Logan Epperson − *Department of Chemistry and Biochemistry, University of Colorado at Colorado Springs, Colorado Springs, Colorado 80918, United States*

Megan Mascarenas − *Department of Chemistry and Biochemistry, University of Colorado at Colorado Springs, Colorado Springs, Colorado 80918, United States*

Complete contact information is available at: https://pubs.acs.org/10.1021/acs.jpca.3c01757

Notes

The authors declare no competing financial interest.

■ ACKNOWLEDGMENTS

This work used the INCLINE cluster at The University of Colorado at Colorado Springs (UCCS). INCLINE is supported by the National Science Foundation (Grant 2017917). L.E. was supported by a graduate teaching fellowship through the graduate school at UCCS. A.M. was supported by startup funds through the College of Letters, Arts, and Sciences at UCCS.

■ REFERENCES

(1) Hirao, H.; Chen, H.; Carvajal, M. A.; Wang, Y.; Shaik, S. Effect of external electric fields on the C−H bond activation reactivity of nonheme iron−oxo reagents. *J. Am. Chem. Soc.* **2008**, *130*, 3319−3327.

(2) Meir, R.; Chen, H.; Lai, W.; Shaik, S. Oriented electric fields accelerate Diels−Alder reactions and selectivity. *ChemPhysChem* **2010**, *11*, 301−310.

(3) Hennefarth, M. R.; Alexandrova, A. N. Heterogeneous intramolecular electric field as a descriptor of Diels−Alder reactivity. *J. Phys. Chem. A* **2021**, *125*, 1289−1298.

(4) Foroutan-Nejad, C.; Marek, R. Potential energy surface and binding energy in the presence of an external electric field: modulation of anion−π interactions for graphene-based receptors. *Phys. Chem. Chem. Phys.* **2014**, *16*, 2508−2514.

(5) Yadav, P.; Rai, P. K.; Mallick, S.; Kumar, P. External electric field to control the Diels−Alder reactions of endohedral fullerene. *Phys. Chem. Chem. Phys.* **2022**, *24*, 11131−11136.

(6) Bhattacharyya, K.; Karmakar, S.; Datta, A. External electric field control: driving the reactivity of metal-free azide−alkyne click reactions. *Phys. Chem. Chem. Phys.* **2017**, *19*, 22482−22486.

(7) Shaik, S.; Ramanan, R.; Danovich, D.; Mandal, D. Structure and reactivity/selectivity control by oriented-external electric fields. *Chem. Soc. Rev.* **2018**, *47*, 5125−5145.

(8) Wang, Z.; Danovich, D.; Ramanan, R.; Shaik, S. Oriented-external electric fields create absolute enantioselectivity in Diels−Alder Reactions: Importance of the molecular dipole moment. *J. Am. Chem. Soc.* **2018**, *140*, 13350−13359.

(9) Wan, M.; Yue, H.; Notarangelo, J.; Liu, H.; Che, F. Deep learning-assisted investigation of electric field−dipole effects on catalytic ammonia synthesis. *JACS Au* **2022**, *2*, 1338−1349.

(10) Aragonès, A. C.; Haworth, N. L.; Darwish, N.; Ciampi, S.; Bloomfield, N. J.; Wallace, G. G.; Diez-Perez, I.; Coote, M. L. Electrostatic catalysis of a Diels-Alder reaction. *Nature* **2016**, *531*, 88−91.
(11) Zheng, C.; Mao, Y.; Kozuch, J.; Atsango, A. O.; Ji, Z.; Markland, T. E.; Boxer, S. G. A two-directional vibrational probe reveals different electric field orientations in solution and an enzyme active site. *Nat. Chem.* **2022**, *14*, 891−897.
(12) Gorin, C. F.; Beh, E. S.; Kanan, M. W. An electric field−induced change in the selectivity of a metal oxide−catalyzed epoxide rearrangement. *J. Am. Chem. Soc.* **2012**, *134*, 186−189.
(13) Huang, X.; Tang, C.; Li, J.; Chen, L.-C.; Zheng, J.; Zhang, P.; Le, J.; Li, R.; Li, X.; Liu, J.; et al. Electric field-induced selective catalysis of single-molecule reaction. *Sci. Adv.* **2019**, *5*, No. eaaw3072.
(14) Li, Z.; Lyu, M.; Jónsson, H.; Rose-Petruck, C. Observation of electric-field-induced liberation of guest molecules from clathrate hydrate. *J. Phys. Chem. Lett.* **2021**, *12*, 10410−10416.
(15) Borca, B.; Michnowicz, T.; Pétuya, R.; Pristl, M.; Schendel, V.; Pentegov, I.; Kraft, U.; Klauk, H.; Wahl, P.; Gutzler, R.; Arnau, A.; Schlickum, U.; Kern, K. Electric-field-driven direct desulfurization. *ACS Nano* **2017**, *11*, 4703−4709.
(16) Alemani, M.; Peters, M. V.; Hecht, S.; Rieder, K.-H.; Moresco, F.; Grill, L. Electric field-induced isomerization of azobenzene by STM. *J. Am. Chem. Soc.* **2006**, *128*, 14446−14447.
(17) Zheng, Q.-N.; Liu, X.-H.; Chen, T.; Yan, H.-J.; Cook, T.; Wang, D.; Stang, P. J.; Wan, L.-J. Formation of halogen bond-based 2D supramolecular assemblies by electric manipulation. *J. Am. Chem. Soc.* **2015**, *137*, 6128−6131.
(18) Zhang, L.; Laborda, E.; Darwish, N.; Noble, B. B.; Tyrell, J. H.; Pluczyk, S.; Le Brun, A. P.; Wallace, G. G.; Gonzalez, J.; Coote, M. L.; Ciampi, S. Electrochemical and electrostatic cleavage of alkoxyamines. *J. Am. Chem. Soc.* **2018**, *140*, 766−774.
(19) Clarys, T.; Stuyver, T.; De Proft, F.; Geerlings, P. Extending conceptual DFT to include additional variables: Oriented external electric field. *Phys. Chem. Chem. Phys.* **2021**, *23*, 990−1005.
(20) Wilson, T. R.; Morgenstern, A.; Alexandrova, A. N.; Eberhart, M. E. Bond bundle analysis of ketosteroid isomerase. *J. Phys. Chem. B* **2022**, *126*, 9443−9456.
(21) Sowlati-Hashjin, S.; Karttunen, M.; Matta, C. F. Manipulation of diatomic molecules with oriented external electric fields: Linear correlations in atomic properties lead to nonlinear molecular responses. *J. Phys. Chem. A* **2020**, *124*, 4720−4731.
(22) Sowlati-Hashjin, S.; Matta, C. F. The chemical bond in external electric fields: Energies, geometries, and vibrational Stark shifts in diatomic molecules. *J. Chem. Phys.* **2013**, *139*, 144101.
(23) Wilson, T. R.; Alexandrova, A. N.; Eberhart, M. E. Electron density geometry and the quantum theory of atoms in molecules. *J. Phys. Chem. A* **2021**, *125*, 10622−10631.
(24) Eberhart, M. E.; Wilson, T. R.; Johnston, N. W.; Alexandrova, A. N. Geometry of charge density as a reporter on the role of the protein scaffold in enzymatic catalysis: Electrostatic preorganization and beyond. *J. Chem. Theor. Comput.* **2023**, *19*, 694−704.
(25) Parr, R. G.; Yang, W. Density functional approach to the frontier-electron theory of chemical reactivity. *J. Am. Chem. Soc.* **1984**, *106*, 4049−4050.
(26) Ayers, P. W.; Yang, W. T.; Bartolotti, L. J. Fukui Function. In *Chemical Reactivity Theory: A Density Functional View*; Chattaraj, P. K., Ed.; CRC Press: Boca Raton, FL, 2009; pp 255−267.
(27) Yang, W.; Mortier, W. J. The use of global and local molecular parameters for the analysis of the gas-phase basicity of amines. *J. Am. Chem. Soc.* **1986**, *108*, 5708−5711.
(28) Bader, R. F. W. Atoms in molecules. *Acc. Chem. Res.* **1985**, *18*, 9−15.
(29) Bader, R. F. W. *Atoms in Molecules: A Quantum Theory*; Clarendon Press: Oxford, U.K., 1990.
(30) Bader, R.; Anderson, S.; Duke, A. Quantum topology of molecular charge distributions. 1. *J. Am. Chem. Soc.* **1979**, *101*, 1389−1395.
(31) Martín Pendás, A.; Costales, A.; Luaña, V. Ions in crystals: The topology of the electron density in ionic materials. I. Fundamentals. *Phys. Rev. B* **1997**, *55*, 4275−4284.
(32) Eberhart, M. A quantum description of the chemical bond. *Philos. Mag. B* **2001**, *81*, 721−729.
(33) Nasertayoob, P.; Shahbazian, S. Revisiting the foundations of the quantum theory of atoms in molecules: Toward a rigorous definition of topological atoms. *Int. J. Quantum Chem.* **2009**, *109*, 726−732.
(34) Morgenstern, A.; Wilson, T.; Miorelli, J.; Jones, T.; Eberhart, M. E. In search of an intrinsic chemical bond. *Comput. Theor. Chem.* **2015**, *1053*, 31−37.
(35) Zadeh, F. H.; Shahbazian, S. Toward a fuzzy atom view within the context of the quantum theory of atoms in molecules: quasi-atoms. *Theor. Chem. Acc.* **2011**, *128*, 175−181.
(36) Heidarzadeh, F.; Shahbazian, S. The quantum divided basins: A new class of quantum subsystems. *Int. J. Quantum Chem.* **2011**, *111*, 2788−2801.
(37) Morgenstern, A.; Eberhart, M. Bond dissociation energies from the topology of the charge density using gradient bundle analysis. *Phys. Scr.* **2016**, *91*, 023012.
(38) Morgenstern, A.; Morgenstern, C.; Miorelli, J.; Wilson, T.; Eberhart, M. E. The influence of zero-flux surface motion on chemical reactivity. *Phys. Chem. Chem. Phys.* **2016**, *18*, 5638−5646.
(39) Morgenstern, A.; Wilson, T. R.; Eberhart, M. E. Predicting chemical reactivity from the charge density through gradient bundle analysis: Moving beyond Fukui functions. *J. Phys. Chem. A* **2017**, *121*, 4341−4351.
(40) Morgenstern, A. Gradient Bundles. In *Advances in Quantum Chemical Topology Beyond QTAIM*; Rodríguez, J. I., Cortés-Guzmán, F., Anderson, J. S. M., Eds.; Elsevier, 2022; Chapter 13.
(41) Geerlings, P.; De Proft, F.; Langenaeker, W. Conceptual density functional theory. *Chem. Rev.* **2003**, *103*, 1793−1874.
(42) Johnson, P. A.; Bartolotti, L. J.; Ayers, P. W.; Fievez, T.; Geerlings, P. Charge Density and Chemical Reactions: A Unified View from Conceptual DFT. In *Modern Charge-Density Analysis*; Gatti, C., Macchi, P., Eds.; Springer: Dordrecht, The Netherlands, 2012; pp 715−764.
(43) Geerlings, P.; Chamorro, E.; Chattaraj, P. K.; De Proft, F.; Gázquez, J. L.; Liu, S.; Morell, C.; Toro-Labbé, A.; Vela, A.; Ayers, P. Conceptual density functional theory: status, prospects, issues. *Theor. Chem. Acc.* **2020**, *139*, 36.
(44) Geerlings, P.; De Proft, F. External fields in conceptual density functional theory. *J. Comput. Chem.* **2023**, *44*, 442−455.
(45) te Velde, G.; Bickelhaupt, F. M.; Baerends, E. J.; Fonseca Guerra, C.; van Gisbergen, S. J. A.; Snijders, J. G.; Ziegler, T. Chemistry with ADF. *J. Comput. Chem.* **2001**, *22*, 931−967.
(46) Johnson, R. D., III, Ed. *NIST Computational Chemistry Comparison and Benchmark Database*, Standard Reference Database 101, release 22. National Institute of Standards and Technology, May 2022. https://cccbdb.nist.gov/ (accessed 2023-03-01).
(47) *ADF*, ver. 2022.1; SCM: Amsterdam, 2022.
(48) Walker, M.; Harvey, A. J. A.; Sen, A.; Dessent, C. E. H. Performance of M06, M06-2X, and M06-HF density functionals for conformationally flexible anionic clusters: M06 functionals perform better than B3LYP for a model system with dispersion and ionic hydrogen-bonding interactions. *J. Phys. Chem. A* **2013**, *117*, 12590−12600.
(49) Wang, Y.; Verma, P.; Jin, X.; Truhlar, D. G.; He, X. Revised M06 density functional for main-group and transition-metal chemistry. *Proc. Natl. Acad. Sci. U.S.A.* **2018**, *115*, 10257−10262.
(50) Limacher, P. A.; Mikkelsen, K. V.; Lüthi, H. P. On the accurate calculation of polarizabilities and second hyperpolarizabilities of polyacetylene oligomer chains using the CAM-B3LYP density functional. *J. Chem. Phys.* **2009**, *130*, 194114.
(51) van Lenthe, E.; Baerends, E. Optimized Slater-type basis sets for the elements 1−118. *J. Comput. Chem.* **2003**, *24*, 1142.

https://doi.org/10.1021/acs.jpca.3c01757
J. Phys. Chem. A 2023, 127, 4682−4694

(52) Hanaway, D. J.; Kennedy, C. R. Automated variable electric-field DFT application for evaluation of optimally oriented electric fields on chemical reactivity. *J. Org. Chem.* **2023**, *88*, 106−115.
(53) Pansini, F. N. N.; de Souza, F. A. L.; Campos, C. T. Molecules under external electric field: On the changes in the electronic structure and validity limits of the theoretical predictions. *J. Comput. Chem.* **2018**, *39*, 1561−1567.
(54) Calvaresi, M.; Martinez, R. V.; Losilla, N. S.; Martinez, J.; Garcia, R.; Zerbetto, F. Splitting CO2 with electric fields: A computational investigation. *J. Phys. Chem. Lett.* **2010**, *1*, 3256−3260.
(55) Franchini, M.; Philipsen, P. H. T.; Visscher, L. The Becke fuzzy cells integration scheme in the Amsterdam Density Functional program suite. *J. Comput. Chem.* **2013**, *34*, 1819−1827.
(56) Rodriguez, J.; Bader, R.; Ayers, P.; Michel, C.; Götz, A.; Bo, C. A high performance grid-based algorithm for computing QTAIM properties. *Chem. Phys. Lett.* **2009**, *472*, 149−152.
(57) Rodriguez, J. An efficient method for computing the QTAIM topology of a scalar field: The electron density case. *J. Comput. Chem.* **2013**, *34*, 681−686.
(58) Tecplot, Inc. *Tecplot 360*. http://www.tecplot.com/ (accessed 2023-05-01).
(59) Wilson, T. *BondalyzerWindows*. https://github.com/twilsonco/BondalyzerWindows (accessed 2023-03-01).
(60) Bulat, F. A.; Chamorro, E.; Fuentealba, P.; Toro-Labbe, A. Condensation of frontier molecular orbital Fukui functions. *J. Phys. Chem. A* **2004**, *108*, 342−349.
(61) Bultinck, P.; Fias, S.; Van Alsenoy, C.; Ayers, P. W.; Carbó-Dorca, R. Critical thoughts on computing atom condensed Fukui functions. *J. Chem. Phys.* **2007**, *127*, 034102.
(62) Sablon, N.; De Proft, F.; Ayers, P. W.; Geerlings, P. Computing Fukui functions without differentiating with respect to electron number. II. Calculation of condensed molecular Fukui functions. *J. Chem. Phys.* **2007**, *126*, 224108.
(63) Bishop, D. M.; Lam, B.; Epstein, S. T. The Stark effect and polarizabilities for a diatomic molecule. *J. Chem. Phys.* **1988**, *88*, 337−341.
(64) Stone, A. *The Theory of Intermolecular Forces*; Oxford University Press: Oxford, U.K., 2013.
(65) Wang, C.; Danovich, D.; Chen, H.; Shaik, S. Oriented external electric fields: Tweezers and catalysts for reactivity in halogen-bond complexes. *J. Am. Chem. Soc.* **2019**, *141*, 7122−7136.
(66) Ayers, P. W.; Morrison, R. C.; Roy, R. K. Variational principles for describing chemical reactions: Condensed reactivity indices. *J. Chem. Phys.* **2002**, *116*, 8731−8744.
(67) Echegaray, E.; Cárdenas, C.; Rabi, S.; Rabi, N.; Lee, S.; Zadeh, F. H.; Toro-Labbe, A.; Anderson, J. S. M.; Ayers, P. W. In pursuit of negative Fukui functions: examples where the highest occupied molecular orbital fails to dominate the chemical reactivity. *J. Mol. Model* **2013**, *19*, 2779−2783.
(68) Melin, J.; Ayers, P. W.; Ortiz, J. V. Removing electrons can increase the electron density: A computational study of negative Fukui functions. *J. Phys. Chem. A* **2007**, *111*, 10017−10019.
(69) Choi, Y. C.; Kim, W. Y.; Park, K.-S.; Tarakeshwar, P.; Kim, K. S.; Kim, T.-S.; Lee, J. Y. Role of molecular orbitals of the benzene in electronic nanodevices. *J. Chem. Phys.* **2005**, *122*, 094706.
(70) Li, Y.; Zhao, J.; Yin, X.; Yin, G. Ab initio investigations of the electric field dependence of the geometric and electronic structures of molecular wires. *J. Phys. Chem. A* **2006**, *110*, 11130−11135.
(71) Rai, D.; Joshi, H.; Kulkarni, A. D.; Gejji, S. P.; Pathak, R. K. Electric field effects on aromatic and aliphatic hydrocarbons: A density-functional study. *J. Phys. Chem. A* **2007**, *111*, 9111−9121.

https://doi.org/10.1021/acs.jpca.3c01757
J. Phys. Chem. A 2023, 127, 4682−4694